Two-step phase shifting interferometry based on orientation selective monogenic filtering

Rishikesh Kulkarni

Department of Electronics and Electrical Engineering, Indian Institute of Technology Guwahati, India.

Pramod Rastogi

Applied Computing and Mechanics Laboratory, Ecole Polytechnique Fédérale de Lausanne, 1015 Lausanne, Switzerland.

Abstract

We propose a phase step estimation algorithm in a two-step phase shifting interferometry setup based on orientation selective adaptive monogenic filtering (AMF). Initially, the AMF algorithm is used for the fringe pattern normalization. A minor modification in the same algorithm performs an orientation selective monogenic filtering which is capable of providing a reliable estimation of phase step. Due to the use of the same algorithm for normalization and phase step estimation, the proposed method offers computational efficiency and simplicity. Simulation and experimental results are provided to demonstrate the suitability of the proposed method in phase demodulation.

Keywords: Two-step phase shifting interferometry, monogenic signal, orientation selective monogenic filter, phase step.

1. Introduction

Optical interferometric measurement techniques such as digital speckle pattern interferometry, shearography, moiré interferometry, and digital holography involve recording of FPs each carrying information on the physical parameters under observation. Fringe pattern (FP) is a sinusoidally varying interference pattern which embeds the whole-field information on the measurand in its phase profile. Therefore, the FP analysis mainly involves phase demodulation. One of the most popular optical configuration for phase measurement is *phase shifting interferometry* (PSI). In this technique,

multiple *phase-shifted* FPs are recorded by introducing pre-defined phase variations in the reference arm of the interferometer under the assumption that the measurand does not vary during the recordings. In general, at least three FPs are essential for a successful phase demodulation. However, due to the presence of environmental disturbances and component tolerances, more than three FP recordings become essential for reliable phase demodulation. Nonetheless, from the perspective of measurement applications, one of the ensuing consequences of these recordings is to impose limitation on the applicability of the PSI technique to the measurement of static paramters only. At the same time, in order to keep other parameters unaltered during phase shifts, the experimental setup needs to be made insensitive to vibrations which is hardly possible in an industrial environment. In order to address these practical issues, a number of PSI algorithms over the years have been reported [1, 2, 3].

Presently, the main research efforts have been in estimating phase steps from only two phase shifted FPs. This overcomes many of the limitations associated with the PSI setup [4, 5, 6, 7, 8, 9, 10, 11, 12, 13, 14, 15, 16, 17, 18, 19, 20, 21]. The PSI algorithms designed in the case for an unknown phase step involve a two step procedure for phase demodulation. First, the phase step between the two FPs is estimated. Subsequently, this estimate is used in the phase demodulation operation. In general, the phase step applied between the two FPs is unknown and which can take any value within $(0, \pi)$. Different algorithms have been reported for the estimation of the unknown phase step. The Fourier transform based method by Kreis et. al. proposes a pointwise demodulation of FPs [4]. A self-tuning (ST) quadrature filter proposed in [5] estimates the unknown phase step before phase demodulation. Vargas et. al. proposed a two-step algorithm for phase demodulation [6] in which a fringe direction map is computed at first using a regularized optical flow (OF) algorithm. Subsequently, the fringe orientated map in association with the spiral phase transform applied to one of the FPs provides a corresponding quadrature FP from which an unambiguous phase estimate can be obtained. The Gram-Schmidth (GS) orthonormalization method [7] applied to the FPs provides orthonormal FPs with which the phase demodulation can be performed easily. Extreme values of interference (EVI) [8] based method is a computationally efficient way of computing the phase step estimate. Apart from these phase demodulation methods,

other phase step estimation algorithms based on two-dimensional continuous wavelet transform [9], quotient of the inner product [12], independent component analysis [15] and polynomial phase fitting and global optimization [17, 19, 20] have been reported.

In this work, we propose a phase shift estimation algorithm in a two-step PSI setup based on orientation selective monogenic filtering of FPs. The two FPs are filtered by a set of complex monogenic filters tuned at specific frequencies. One real and two imaginary components of the filtered monogenic FP provides the local amplitude and phase information associated with these frequencies. This information derived at different frequency values is utilized for a reliable phase shift estimation.

2. Proposed Method

In a phase shifting interferometric setup, two phase shifted fringe patterns (FPs) can be represented as

$$I_k(\boldsymbol{r}) = a_k(\boldsymbol{r}) + b_k(\boldsymbol{r})\cos\left[\phi(\boldsymbol{r}) + \alpha_k\right], \text{ for } k = 1, 2. \tag{1}$$

where, $\boldsymbol{r} = [x, y]^T$ indicates the pixel spatial coordinates in the FP lattice; $a_k(\boldsymbol{r})$ and $b_k(\boldsymbol{r})$ represent the background intensity and the fringe amplitude, respectively; $\phi(\boldsymbol{r})$ is the phase encoded in the FP. In general, the phase shifts (α_k) associated with the two FPs are considered as $\alpha_1 = 0$ and $\alpha_2 = \alpha$. In the proposed method, the FPs are first normalized using the adaptive monogenic filtering based technique described in [22]. Subsequently, a modified monogenic filtering is performed on the normalized FPs to obtain the phase estimate. The procedure of fringe normalization is outlined in the following section.

2.1. Fringe Normalization Based on Adaptive Monogenic Filter

The monogenic filtering utilizes the local single frequency sinusoidal nature of the FP. In the neighborhood around a pixel $\boldsymbol{r}'$ the fringe signal can be represented as

$$I(\boldsymbol{r}) = A\cos\left[\boldsymbol{\omega}_0^T(\boldsymbol{r} - \boldsymbol{r}') + \phi\right], \tag{2}$$

where $\boldsymbol{\omega}_0 = [\omega_x, \omega_y]^T$ represents the local frequency vector. Considering such a fringe model, a narrow-band low pass filter tuned at $\boldsymbol{\omega}_0$ is able to effectively remove the

noise from the fringe signal. Apart from noise filtering, an equivalent analytic signal can be derived using a complex quadrature filter to obtain the amplitude and phase information. The complex valued analytic signal corresponding to the FP in Eq. (1) can be expressed as

$$I_c(\boldsymbol{r}) = A(\boldsymbol{r}) \exp\{j\,[\phi(\boldsymbol{r}) + \alpha]\} \quad j = \sqrt{-1}. \tag{3}$$

The derivation of analytic signal in Eq. (3) from the two dimensional sinusoidal signal in Eq. (1) is not straightforward. We need to consider the isotropic generalization of the analytic signal, the *monogenic signal*, to obtain the local amplitude and phase information [23]. The adaptive monogenic filtering based fringe denoising and normalization has been proposed in [22]. In this method, the FP is filtered using a set of isotropic filters tuned at a certain number of frequencies. The output signals of these filters are combined in such a manner that a denoised and normalized FP is obtained. The fringe normalization procedure is described below:

1. A bell-shaped function is used as an isotropic filter $H(\boldsymbol{\omega})$ tuned at frequency ω_0 in [22]. In the present work, we propose to use a log-Gabor filter given as

$$H(\boldsymbol{\omega}) = \exp\left(-\frac{\left(\log\left(\frac{||\boldsymbol{\omega}||}{\omega_0}\right)\right)^2}{2\left(\log\left(\sigma_0\right)\right)^2}\right), \tag{4}$$

   where σ_0 is a shape parameter which decides the bandwidth of the filter pass-band. The advantage of using this band pass filter is that its response at $\boldsymbol{\omega} = 0$ is always zero which ensures the filtering of background intensity.
2. The output of log-Gabor filter provides the real part of the analytic image corresponding to the FP. Since the fringe image is a two-dimensional signal, two imaginary parts of the monogenic signal, one for each direction (x and y), need to be computed. The *Riesz transform*, generalization of the *Hilbert transform* is used for this purpose. Note that one real (filtered FP) and two imaginary signals constitute the one even and two odd components of the monogenic signal, respectively.
3. To obtain the one real and two imaginary components of the monogenic signal, the fringe signal is passed through three filters, one even (See Eq. (4)) and two

odd filters given as

$$H_{o1}(\boldsymbol{\omega}) = j\frac{\omega_x}{||\omega||}H(\boldsymbol{\omega})$$
$$H_{o2}(\boldsymbol{\omega}) = j\frac{\omega_y}{||\omega||}H(\boldsymbol{\omega}). \quad (5)$$

Since this filtering is performed in the Fourier domain, the computation of filtered signal components in the spatial domain involve three inverse Fourier transform operations. However, this number can be reduced to two by considering a *complex odd filter* defined as [23]

$$H_o(\boldsymbol{\omega}) = H_{o1}(\boldsymbol{\omega}) + jH_{o2}(\boldsymbol{\omega})$$
$$= \frac{j\omega_x - \omega_y}{||\omega||}H(\boldsymbol{\omega}) \quad (6)$$

Once the FP is filtered using this complex filter, the real and imaginary part of the filtered output are in fact the two odd signal components. This saves one Fourier transform operation than that required in the method presented in [23].

4. Let $I_e(\boldsymbol{r})$ and $I_{o1}(\boldsymbol{r}) + jI_{o2}(\boldsymbol{r})$ represent the output of filters $H(\boldsymbol{\omega})$ and $H_o(\boldsymbol{\omega})$, respectively. Thus, $[I_e(\boldsymbol{r}), I_{o1}(\boldsymbol{r}), I_{o2}(\boldsymbol{r})]^T$ represents the monogenic image. The local amplitude and local phase map are computed as

$$|I_o(\boldsymbol{r})| = \sqrt{I_{o1}^2(\boldsymbol{r}) + I_{o2}^2(\boldsymbol{r})} \quad (7)$$
$$A(\boldsymbol{r}) = \sqrt{I_e^2(\boldsymbol{r}) + I_o^2(\boldsymbol{r})} \quad (8)$$
$$\phi(\boldsymbol{r}) = \arctan\left(\frac{|I_o(\boldsymbol{r})|}{I_e(\boldsymbol{r})}\right) \quad (9)$$

Note that, Eqs. (8) and (9), respectively, provide the local amplitude and local phase information associated with the filter tuned at a particular frequency $\boldsymbol{\omega_k}$. The adaptive fringe filtering is performed using K number of filters with overlapping passbands. Accordingly, we represent the filtered fringe signal and the local fringe amplitude as $I_e^{(k)}(\boldsymbol{r})$ and $A^{(k)}(\boldsymbol{r})$, respectively, corresponding to the kth filter.

5. Based on the filter outputs computed in the previous step, fringe normalization is performed as follows,

$$I_n(\boldsymbol{r}) = \frac{\sum_{k=1}^{K} w^{(k)}(\boldsymbol{r}) I_e^{(k)}(\boldsymbol{r})}{\sum_{k=1}^{K} w^{(k)}(\boldsymbol{r}) A^{(k)}(\boldsymbol{r})}. \quad (10)$$

The weights $w^{(k)}(\boldsymbol{r})$ are obtained as

$$w^{(k)}(\boldsymbol{r}) = \left(\frac{A^{(k)}(\boldsymbol{r})}{A_{max}(\boldsymbol{r})} \right)^{p}, \tag{11}$$

where $A_{max}(\boldsymbol{r}) = \max_k A^{(k)}(\boldsymbol{r})$; p is a positive constant and it is set $p = 10$ as suggested in [22].

6. In the implementation of Eq. (4), we set $\sigma_0 = 0.2$. The center frequencies (ω_k) of K filters are equispaced in the range of $[\pi/30, \pi/2]$ radians. We set $K = 15$ in all the simulation and experimental examples presented in this paper.

2.2. Phase Shift Estimation from the Normalized Fringe Patterns

Upon normalization, the FPs in Eq. (1) can be represented as,

$$I_k^{(n)}(\boldsymbol{r}) = \cos\left[\phi(\boldsymbol{r}) + \alpha_k\right], \text{ for } k = 1, 2. \tag{12}$$

In order to estimate the value of α, we propose to use the same monogenic filter described in the previous subsection with a minor modification. The isotropic filter in the frequency domain in Eq. (4) is modified as

$$H_\alpha(\boldsymbol{\omega}) = G(\boldsymbol{\omega}) H(\boldsymbol{\omega}), \tag{13}$$

where $G(\boldsymbol{\omega})$ represents a binary mask in the frequency domain. The value of $G(\boldsymbol{\omega})$ is 1 only in one quadrant and 0 otherwise. The masked isotropic filter in the frequency domain retains fringes with certains orientations only and filters out remaining fringes. For example, consider a normalized FP in Fig.1a where fringes with all possible orientations are present. This FP is filtered using the monogenic filter defined using $H_\alpha(\boldsymbol{\omega})$. Figures 1b and 1c show the magnitude plots of one of $H(\boldsymbol{\omega})$ and $H_\alpha(\boldsymbol{\omega})$ filters, respectively. The filtered FP in Fig. 1d indicates the orientation selective filtering. The local amplitude and phase maps are shown in Figs. 1e and 1f, respectively.

Monogenic fringe signal magnitude and phase values are computed for each one of the selected K number of filters. At each pixel, fringe signal with the maximum magnitude is selected for further processing. Let us represent this signal as $I_k^{(f)}(\boldsymbol{r})$, which is the complex valued analytic representation of the original real-valued fringe

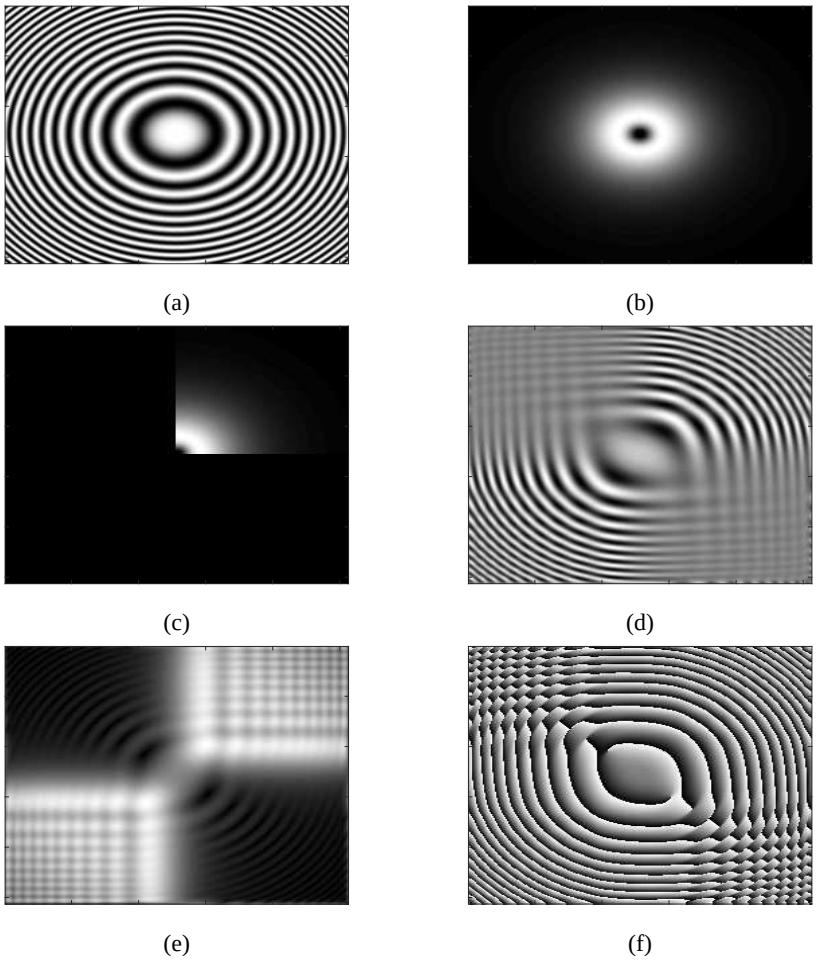

Figure 1: Simulation Example: (a) normalized fringe pattern (b) and (c) magnitude plots of $H(\boldsymbol{\omega})$ and $H_\alpha(\boldsymbol{\omega})$, respectively. (d) Orientation selective filtered fringe signal. (e) and (f) Magnitude and phase plots of filtered fringe signal, respectively.

signal. According to Eq. (3), the complex-valued FPs can be expressed as,

$$I_1^{(f)}(\boldsymbol{r}) = A_1(\boldsymbol{r}) \exp\{j[\phi(\boldsymbol{r})]\} \tag{14}$$

$$I_2^{(f)}(\boldsymbol{r}) = A_2(\boldsymbol{r}) \exp\{j[\phi(\boldsymbol{r}) + \alpha]\} \tag{15}$$

Equations (14) and (15) suggest that the phase step estimate can be obtained as

$$I_d(\boldsymbol{r}) = I_2^{(f)}(\boldsymbol{r}) \left(I_1^{(f)}(\boldsymbol{r})\right)^* \tag{16}$$

$$\alpha(\boldsymbol{r}) = \angle\{I_d(\boldsymbol{r})\} \tag{17}$$

In order to obtain reliable phase step estimate, we consider only those pixels where $|I_d(\boldsymbol{r})|$ is above a certain threshold value. We set this threshold as $0.3|I_d(\boldsymbol{r})|_{max}$. Using the phase step estimates at these selected pixels, a histogram is computed. The phase step value observed at a maximum number of pixels is considered to be the phase step estimate $\hat{\alpha}$. Finally, the phase estimate is computed as

$$\hat{\phi}(\boldsymbol{r}) = \arctan\left[\frac{I_1^{(n)}(\boldsymbol{r})\cos(\hat{\alpha}) - I_2^{(n)}(\boldsymbol{r})}{I_1^{(n)}(\boldsymbol{r})\sin(\hat{\alpha})}\right] \tag{18}$$

For the FP example considered in Fig. 1, the simulation was performed with $\alpha = 1\ rad$. The above described method is used to estimate the phase step and subsequently the phase map. The phase step is accurately estimated from the histogram of estimated phase steps obtained at selected pixels as shown in Fig. 2a. Figure 2b shows the phase map computed using this phase step estimate.

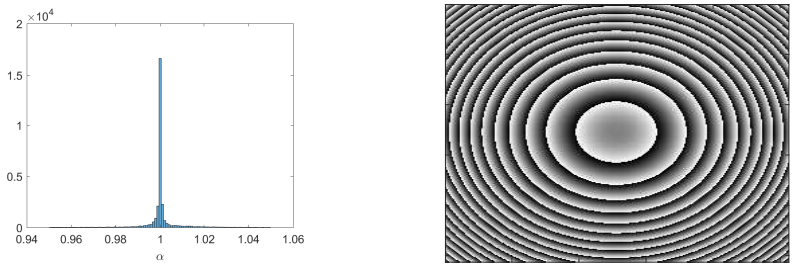

(a) (b)

Figure 2: a) Histogram of the estimated phase step at selected pixels. Phase step values are in radians. b) Estimated phase map.

3. Simulation Results

A simulation example is provided for the phase demodulation of FPs shown in Fig. 3 which were simulated with a phase step of α = 1 rad at signal to noise ratio

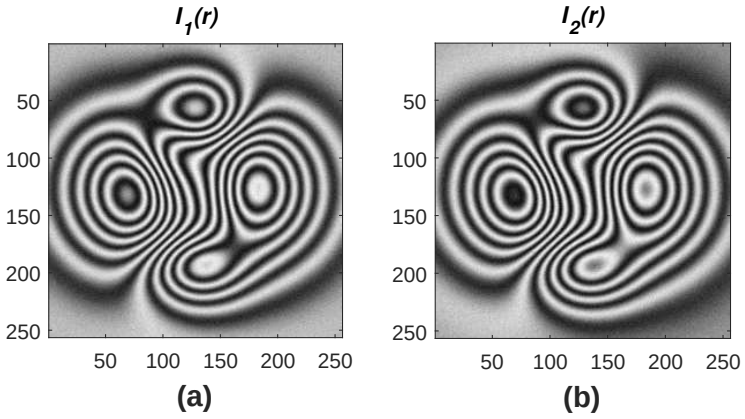

Figure 3: Phase shifted FPs of size 256×256 simulated with $\alpha = 1$ at SNR = 20 dB.

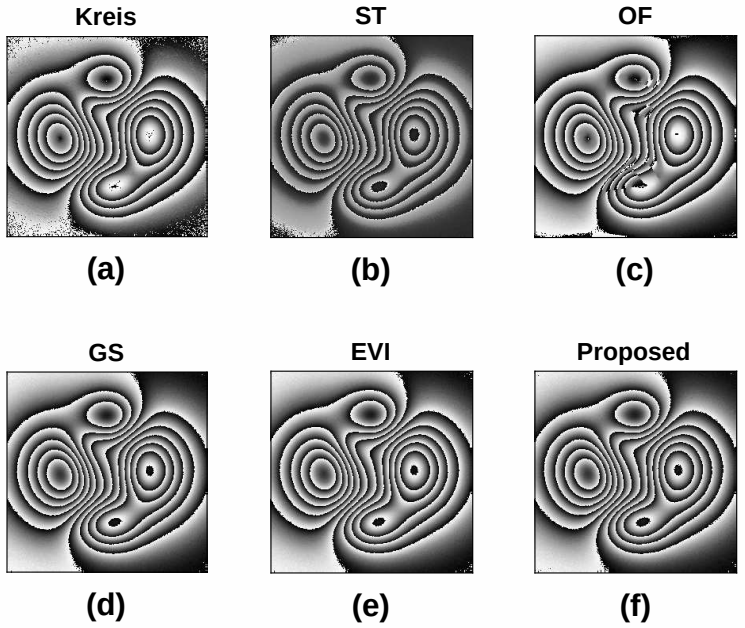

Figure 4: Estimated phase maps from the phase shifted FPs shown in Fig. 3 using (a) Kries (b) ST (c) OF (d) GS (e) EVI and (f) the proposed method.

(SNR) of 20 dB. The fringe amplitude was set as $b(x,y) = 25 \cdot \exp\{-(\boldsymbol{r}^2/5e4)\}$. In the implementation of the proposed method, we have set $K = 15$, $\sigma_0 = 0.2$, $\boldsymbol{\omega}_{min} = \pi/30$ and $\boldsymbol{\omega}_{max} = \pi/5$, for all of the simulation and experimental study. Figure 4 shows the phase maps estimated using the Kries, ST, OF, GS, EVI and the proposed method. It

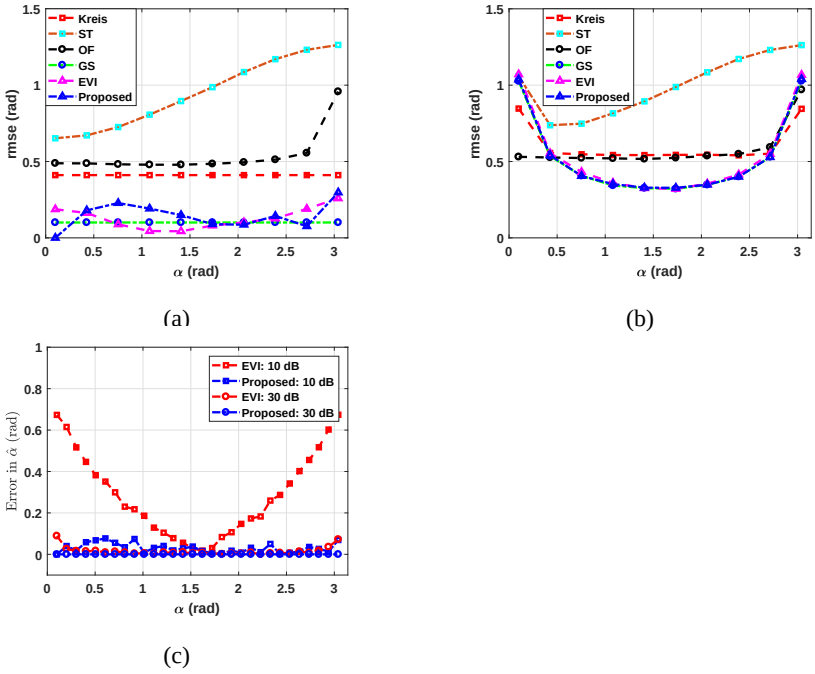

Figure 5: Root mean square error in the estimation of phase computed using the Kries, ST, OF, GS, EVI and the proposed method in function of α at (a) SNR = ∞ dB and (b) SNR = 20 dB. (c) Error in the estimation of phase step computed using the EVI and the proposed method in function of α at SNR = 10 and 30 dB.

has been found that while the Kries, ST and OF methods provided inaccurate phase estimates, the GS, EVI and the proposed method resulted in reliable phase estimates. Root Mean Square Errors (RMSE)s in phase estimation are computed, for the fringe pattern example shown in Fig. 4, in function of α at SNR = ∞ dB and 20 dB, as shown Figs. 5a and 5b, respectively. Accurate phase estimates for a wide range of α values are obtained using the GS, the EVI and the proposed method. Albeit the main purpose of FP analysis being phase estimation, the proposed method is developed with the main objective of accurate phase step estimation. Consequently, the performance of the proposed algorithm is also evaluated for the estimation of phase step. Errors in the phase step evaluation using the EVI and the proposed method are compared in Fig. 5c at SNR = 10 dB and 30 dB which indicates a higher noise tolerance of the proposed method compared to the EVI method over the entire range of α.

4. Experimental Results

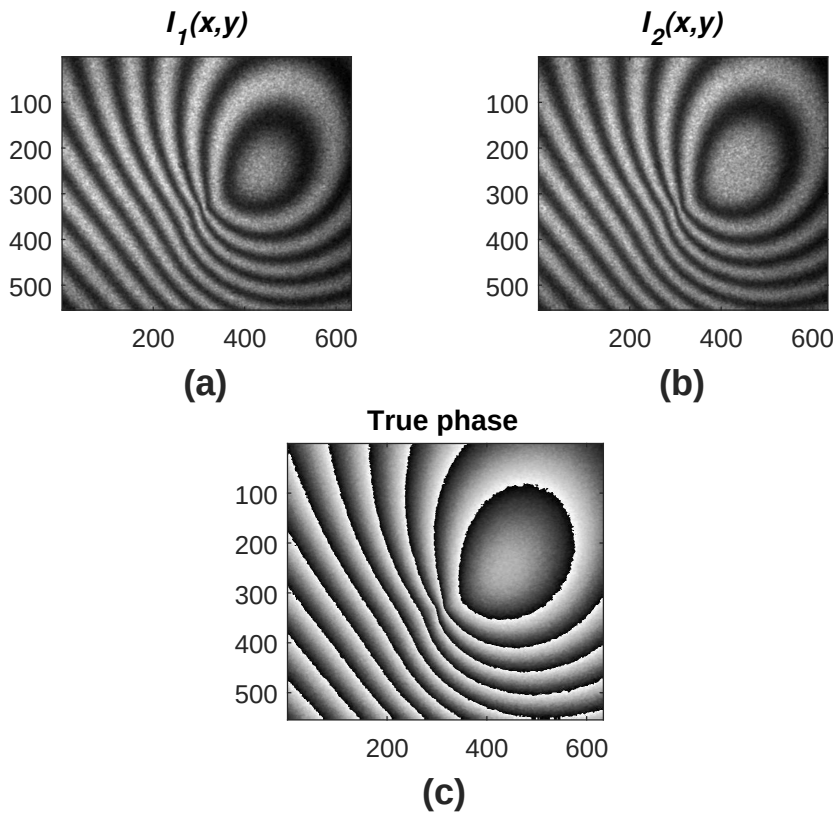

Figure 6: (a) and (b) Two phase-shifted FPs recorded in a classical holographic interferometric setup corresponding to out-of-plane deformation of an aluminum plate. (c) The reference true phase computed using the Schwider-Hariharan (5-step) phase shifting algorithm.

Experimental validation of the proposed method is performed using the FPs recorded in a classical holographic interferometry setup. Two out of total five phase shifted FPs corresponding to the out-of-plane deformation of an aluminum plate are shown in Figs. 6(a) and (b). For reference, the FPs were demodulated using the five-frame Schwider-Hariharan algorithm [24, 25]. The estimated phase shown in Fig. 6(c) is considered to be the true phase map.

The phase estimated obtained using the Kries, ST, OF, GS, EVI and the proposed method are shown in Fig. 7. The errors in the wrapped phase estimation with respect

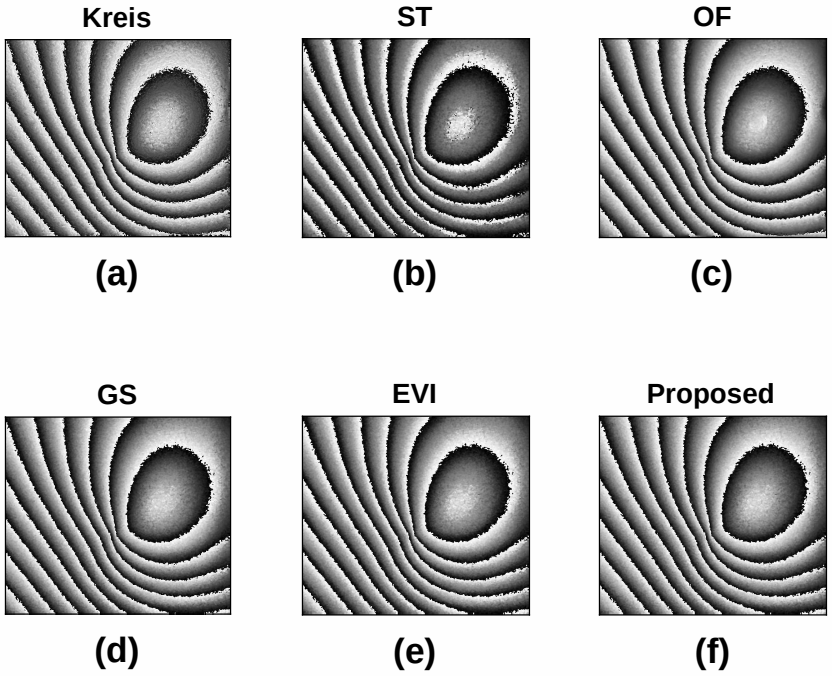

Figure 7: Estimated phase maps from the phase shifted FPs shown in Fig. 6 using (a) Kries (b) ST (c) OF (d) GS (e) EVI and (f) the proposed method.

to Fig. 6(c) are shown in Fig. 8. The phase estimation error variances (σ) computed for each method are also provided in the figure. We have included this figure in our revised manuscript. The estimated phase step by the EVI method and the proposed method were 0.7948 *rad* and 0.9602 *rad*, respectively. The true phase step applied between the two fringe patterns was $\pi/3 = 1.0472$ *rad*. This results shows that the phase step estimated with the proposed method is more accurate compared to the EVI method. The experimental results demonstrate the practical feasibility of the proposed method.

5. Discussion

The proposed method provides reliable phase step estimation over a wide range of phase step values. However, for the phase step close to 0 and π, since the two fringe patterns are almost identical, the accuracy of the phase step estimation using the

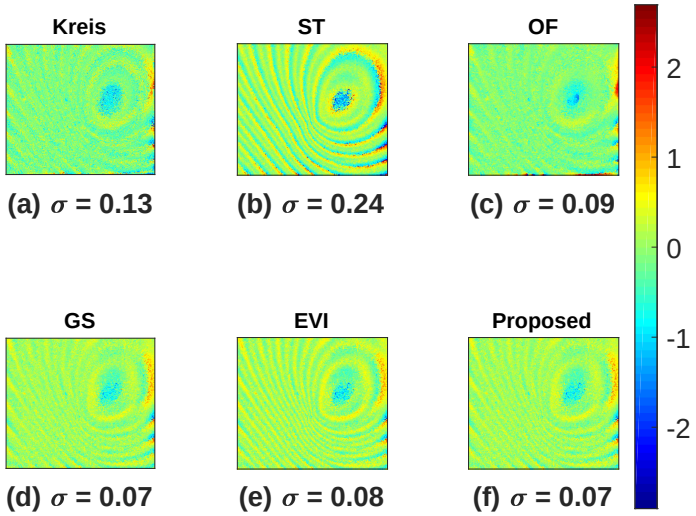

Figure 8: Error in the estimated phase maps with respect to Fig. 6(c) computed using (a) Kries (b) ST (c) OF (d) GS (e) EVI and (f) the proposed method. σ represents error variance. All values are in radians.

proposed method is low. However, this is true with most of the two-step phase shifting interferometry algorithms. The simulation and experimental results demonstrated that the performance of the proposed method is independent of fringe density. However, it is important to note that the performance depends on the appropriate selection of range of center frequencies $\boldsymbol{\omega}_{min}$ and $\boldsymbol{\omega}_{max}$. Thus, some apriori knowledge on the fringe frequency is beneficial. At the same time, if the computation time is not of much concern, then a wide range of center frequencies for the monogenic filters can be selected. Since the two dimensional signal model in Eq. (3) takes into account the local fringe amplitude, the proposed method provides information on the fringe amplitude variation as well. Thus, its performance in the phase step estimation remain unaffected by fringe amplitude modulation.

6. Conclusion

A noise robust phase step estimation algorithm is proposed for a two-step phase shifting interferometry setup. A simple modification of the adaptive monogenic filtering algorithm allows to perform orientation selective filtering of fringe patterns. Phase step estimation can be derived from such filtered fringe patterns. The simulation results exhibit the capability of the proposed algorithm in estimating the phase step over a wide range of its values. The noise robust performance of proposed algorithm is also validated. Finally, the experimental results demonstrate the practical feasibility of the proposed method.

References

[1] Servin M, Quiroga J A, Padilla M Fringe Pattern Analysis for Optical Metrology: Theory, Algorithms, and Applications. Wiley-VCH; 2014.

[2] Kulkarni R, Rastogi P. Phase estimation: temporal fringe analysis. In: Single and multicomponent digital optical signal analysis, IOP Publishing; 2017, p.8-1 to 8-31.

[3] Li J, Zhong L, Liu S, Zhou Y, Xu J, Tian J and Lu X. An advanced phase retrieval algorithm in N-step phase-shifting interferometry with unknown phase shifts. Scientific Reports 2017;7:44307.

[4] Kreis T M, Jueptner W P. Fourier transform evaluation of interference patterns: demodulation and sign ambiguity. Proc. SPIE 1553 1992;263-273.

[5] Vargas J, Quiroga J A, Belenguer T, Servín M, Estrada J C. Two-step self-tuning phase-shifting interferometry. Opt Exp 2011;19(2):638–648.

[6] Vargas J, Quiroga J A, Sorzano C O, Estrada J C, Carazo J M. Two-step interferometry by a regularized optical flow algorithm. Opt Lett 2011;36(17):3485–3487.

[7] Vargas J, Quiroga J A, Sorzano C O, Estrada J C, Carazo, J M. Two-step demodulation based on the Gram-Schmidt orthonormalization method. Opt Lett 2012;37(3):443–445.

[8] Deng J, Wang H, Zhang F, Zhang D, Zhong L, Lu X. Two-step phase demodulation algorithm based on the extreme value of interference. Opt Lett 2012;37(22):4669–4671.

[9] Ma J, Wang Z, Pan T. Two-dimensional continuous wavelet transform algorithm for phase extraction of two-step arbitrarily phase-shifted interferograms. Opt Lasers Eng 2014;55:205–211.

[10] Trusiak M, Patorski K. Two-shot fringe pattern phase-amplitude demodulation using Gram-Schmidt orthonormalization with Hilbert-Huang pre-filtering. Opt Exp 2015;23(4):4672–4690.

[11] Luo C, Zhong L, Sun P, Wang H, Tian J, Lu X. Two-step demodulation algorithm based on the orthogonality of diamond diagonal vectors. Appl Phys B 2015;119(2):387–391.

[12] Niu W, Zhong L, Sun P, Zhang W, Lu X. Two-step phase retrieval algorithm based on the quotient of inner products of phase-shifting interferograms. J Opt 2015;17(8):085703.

[13] Maciek W, Zofia S, Krzysztof P. Two-frame tilt-shift error estimation and phase demodulation algorithm. Opt Lett 2015;40:3460-3463.

[14] Rivera M, Dalmau O, Gonzalez A, Hernandez-Lopez F. Two-step fringe pattern analysis with a Gabor filter bank. Opt Lasers Eng 2016;85:29–37.

[15] Xu X, Shou J, Lu X, Yin Z, Tian J, Li D, Zhong L. Independent component analysis based two-step phase retrieval algorithm. J Opt 2016;18:105701(7pp).

[16] Chao T, Shengchun L. Two-frame phase-shifting interferometry for testing optical surfaces. Opt Exp 2016;24:18695-18708.

[17] Chao T, Shengchun L. Demodulation of two-shot fringe patterns with random phase shifts by use of orthogonal polynomials and global optimization. Opt Exp 2016;24:3202-3215.

[18] Dalmau O, Rivera M, Gonzalez A. Phase shift estimation in interferograms with unknown phase step. Opt Comm 2016;372:37-43.

[19] Chao T, Shengchun L. Phase retrieval in two-shot phase-shifting interferometry based on phase shift estimation in a local mask. Opt Exp 2017;25:21673-21683.

[20] Kulkarni R, Rastogi P. Two-step phase demodulation algorithm based on quadratic phase parameter estimation using state space analysis. Opt Lasers Eng 2018;110:41-46.

[21] Dominika S, Maciej T, Krzysztof P. Evaluation of adaptively enhanced two-shot fringe pattern phase and amplitude demodulation methods. Appl Opt 2017;56:5489-5500.

[22] J. A. Guerrero, J. L. Marroquin, M. Rivera, and J. A. Quiroga, Adaptive monogenic filtering and normalization of ESPI fringe patterns, Opt. Lett. 30 (2005) 3018-3020. https://doi.org/10.1364/OL.30.003018

[23] C.P. Bridge, Introduction to the Monogenic Signal (2017). https://arxiv.org/abs/1703.09199

[24] Schwider J, Burow R, Elssner K E, Grzanna J, Spolaczyk R, Merkel K. Digital wave-front measuring interferometry: some systematic error sources. Appl Opt 1983;22:3421-3432.

[25] Hariharan P, Oreb B F, Eiju T. Digital phase-shifting interferometry: a simple error-compensating phase calculation algorithm. Appl Opt 1987;26:2504-2506.